The influence of the pore structure on the moisture transport in lime plaster-brick systems as studied by NMR

Construction and Building Materials 142 (2017) 395–409

Contents lists available at ScienceDirect

Construction and Building Materials

journal homepage: www.elsevier.com/locate/conbuildmat

The influence of the pore structure on the moisture transport in lime plaster-brick systems as studied by NMR

Cristiana Nunes [a,*], Leo Pel [b], Jiří Kunecký [a], Zuzana Slížková [a]

[a] Institute of Theoretical and Applied Mechanics, Prosecká 809/76, 190 00 Prague, Czech Republic
[b] Department of Applied Physics, Eindhoven University of Technology, P.O. Box 513, 5600 MB Eindhoven, The Netherlands

HIGHLIGHTS

- NMR is a powerful method for simultaneously analysing the porous structure and the moisture transport in masonry systems.
- The water-repellent plaster inhibited the drying of the brick.
- The inhibition of drying by the water-repellent mortar was assigned to the interruption of liquid transport.
- The NMR-T_2 relaxation technique distinguished different pore size geometries in the specimens at a precise position.

ARTICLE INFO

Article history:
Received 19 May 2016
Received in revised form 20 February 2017
Accepted 10 March 2017
Available online 19 March 2017

Keywords:
Drying
Moisture transport
NMR
Pore water distribution
Plaster
Brick
Lime
Metakaolin
Water-repellent
Linseed oil

ABSTRACT

This paper presents an experimental analysis of the porous structure and drying kinetics of lime-based plasters and plaster-brick systems using different methods. The effect of adding a water-repellent admixture (linseed oil) to the plasters was also evaluated. Nuclear Magnetic Resonance (NMR) was used to measure moisture profiles during drying of mono-material plaster specimens and of specimens constituted by the same plasters applied on fired-clay brick. NMR transverse relaxation time was used to examine the pore water distribution. The NMR moisture profiles showed that the drying behaviour of the water-repellent mono-plasters differs slightly from the reference, but when applied on brick, it significantly hinders the drying of the substrate. The results indicated that the addition of linseed oil to the lime plaster has negatively influenced the bonding process and created an hydraulic resistivity for the moisture to flow from the brick to the plaster during drying. This phenomena was mainly atributed to three factors: i) hydrophobization of part of the mortar pores; ii) the development of air bubbles related to entrained air during the mixing process; and iii) the mismatch between the physical-chemical properties of both systems, namely the different pore network and surface energy, which seems to affect the interpenetration of both porous layers.

1. Introduction

Currently, lime has become one of the principal materials used in conservation and restoration of historic buildings. Lime is probably the most versatile binder available and can be modified to suit a range of diverse uses and exposures [1]. Lime plasters or renders are commonly utilised for the repair of built heritage, thanks to their compatibility with traditional masonry materials, and to the fact that they favour liquid migration to the surface, thereby preventing the underlying masonry from degradation processes associated with dampness. However, often in practice, there is a rapid loss of cohesion of repair lime-based mortars with similar composition to the historic ones when exposed to weathering phenomena involving water transport. The presence of water is a necessary condition for many degradation processes, e.g. freeze/thaw cycles, salt crystallisation cycles (and salt related hygroscopic moisture absorption), dissolution and leaching, bio-deterioration [2]. To counteract moisture-related issues in building materials, there is increased research interest on the effect of mixing water-repellent additives in lime mortars to improve its durability [3–5]. Water-repellent admixtures for mortars (added in the mortar bulk) and surface treatments have been used in buildings since the classical era, and vegetable oils were one of the most commonly utilised substances [6]. All the ancient documents mentioning the use of oils in mortars report or recommend its application in severe weathering conditions involving water transport

* Corresponding author.
E-mail addresses: nunes@itam.cas.cz (C. Nunes), l.pel@tue.nl (L. Pel), kunecky@itam.cas.cz (J. Kunecký), slizkova@itam.cas.cz (Z. Slížková).

http://dx.doi.org/10.1016/j.conbuildmat.2017.03.086
0950-0618/

(e.g. Pliny the Elder, Vitruvius, Alberti), but the recipes and application techniques are not specified. The few existing research studies on the use of vegetable oils as admixtures for lime-based mortars indicate very different properties according to the type of oil and binder combined, e.g. [7–10]. Therefore, it is important to investigate the effect of each specific type of oil. Linseed oil was the admixture selected for designing the lime-based mortars in this study owing to its worldwide availability and promising results obtained in a previous study [11]. To tackle the problem of low mechanical strength that characterises air lime mortars, and given the possible negative effect that the addition of oil may induce in the hardening reactions [11], the present study encompasses a mixture of lime and metakaolin. The hereby designated metakaolin corresponds to burnt Czech clay shale [12]; besides being an available material in the country, it was selected considering previous studies reporting its pozzolanic potential [13].

One of the drawbacks that can arise from applying water-repellent mortars in old masonry is that they can hinder capillary water transport and lower the evaporation flux; in many cases, secondary damages after restoration interventions have to do with the use of materials that alter the drying mechanisms of the masonry [14]. However, there is lack of scientific research on the performance of plasters/renders with water-repellent admixtures, particularly regarding their drying behaviour. It is well established in the scientific literature [15] that drying under constant external conditions occurs in two distinct stages, often called the constant drying rate period (stage I) and the falling drying rate period (stage II). From an experimental approach, for most types of porous materials, in stage I, also called constant-rate period, the moisture content decreases more or less linearly with time. In stage II the drying rate falls, which finds expression in the concave form of the drying curve (the evaporation front recedes into the material) [16]. These experiments have been mostly carried out in porous media that are hydrophilic [17].

The aim of this study is the characterisation of the porous structure of lime-based plasters as well as its influence on their drying behaviour, and to evaluate the effect of linseed oil, a traditional water-repellent admixture, on the drying kinetics of the plasters. The water-repellency degree of the plasters used in this research has been previously investigated by determining the rate of water absorption by capillarity [18]; the water absorption coefficient was reduced in ca. 98% and 83% when oil was added to lime and lime-metakaolin plasters, respectively. Given that many parts of buildings are often built up of layers of different materials with different pore space properties, in addition to the study of single materials, it is important to investigate the moisture transport in combinations of materials. Various enlightening studies have been done on the moisture transport across cement based mortars applied on brick using NMR [19–23]. Very few NMR studies [14,24] have been done on the moisture transport in lime-based mortars combined with other materials. Hence, it is also an aim of this study to analyse the moisture transport across lime-based plasters applied on another traditional material. To this end, lime and lime-metakaolin single plaster specimens and specimens constituted by the same plasters applied on fired-clay brick were produced in the laboratory and the properties connected with the presence and movement of water were investigated. Mercury intrusion porosimetry (MIP), optical (OM) and scanning electron microscopy (SEM), and NMR were used to study synergistically the pore-space properties of the samples.

MIP is one of the most used techniques in building materials' research for determining the pore size distribution. However, the calculation of the pore size distribution from MIP data results in systematic deviations from reality, as it reflects the physics of how mercury intrudes into the material and is not controlled by the actual sizes of the pores [25]. If the MIP technique limitations are taken into account, the technique can still be very useful for the characterisation of porous structures [26]. The main advantage of this technique is the wide range of pore sizes that can be measured, but it is problematic to interpret the data as an absolute representation of the pore size distribution, especially with respect to the coarsest pores [27]. The direct observation of the porous structure of the materials with microscopy techniques can help in overcoming some of the MIP limitations. Different pore types (and their spatial distribution) can be distinguished: capillary pores are found within the binder and at aggregate/binder interfaces, coarse pores are generally formed by entrapped or entrained air – entrapped air pores are irregular in shape and distribution whereas entrained air voids are round (bubble-like) and are formed by introduction of admixtures (surfactants) [28]. Moreover, microscopy techniques enable the visualisation of cracks and the study of the Interstitial Transition Zone (ITZ), the bonding and possible reaction rims between aggregates, bricks or building stone, and mortar [28]. The main drawbacks of the use of microscopy techniques are with the sample size and its representativeness, the disturbance of the sample during preparation as well as the necessary experience required for evaluating the results [29]. NMR can be used to determine transient moisture profiles nondestructively and with high spatial resolution, as it is directly related to the amount of hydrogen nuclei, unlike gamma or neutron attenuation methods [30]. As it is further described (Section 2.2.3), NMR can also give additional information by measuring simultaneously the so-called transverse relaxation time (T_2) of water in the materials. Not only the total moisture content is measured, but also the distribution of water in the pores [31]. The NMR equipment used in this study offers the possibility to determine the time evolution of one-dimensional moisture profiles in a large variety of materials. A drawback of the method is the reduction of T_2 in materials containing large amounts of paramagnetic ions (e.g. Fe), which is the case of inorganic building materials like brick and mortar. These properties present special demands on the strategy of the measurements and the hardware performance [30]. In this study, the aim of combining the data obtained with MIP, microscopy techniques, and NMR is to advance the knowledge on the pore space properties and on how moisture moves in the materials during drying.

2. Materials and experimental methods

2.1. Sample preparation

The plasters were prepared with aerial lime, classified as CL 90 S according to EN4591 [32], and pure siliceous sand with controlled granulometry (particle size distribution between 0.1 and 0.5 mm, generally exhibiting angular to sub-angular shape). Linseed oil extracted by the cold press method from flax seeds (supplied by GRAC s.r.o.) was used as a water-repellent admixture. The mixing procedure has been previously determined [18] and consists of blending the oil in the dried mixture of binder and aggregate manually and then adding water and blending the mixture for 3 min in an automatic mixer at low speed; the composition of the mixtures is given in Table 1. The amount of kneading water was pre-determined with the aim of achieving the same consistency in both mixes (reference mixtures and mixtures with oil) with the flow table test [33]; the diameter of the fresh plaster measured on the flow table was ca. 145 ± 3 mm. The mono-plaster specimens were prepared in cylindrical moulds of 15 mm diameter and 35 mm in length using a piston to compact them. The samples were demoulded after one day and were kept for six days in a chamber with 90% relative humidity (RH) at room temperature.

Table 1
Mono-plaster and plaster-brick specimens' identification and composition by weight.

Plaster code	Plaster-brick code	Composition	Binder:aggregate ratio	Amount of oil (%)	Water:binder ratio
L	LB	Lime:Sand	1:3	–	1.01
LO	LOB	Lime:Sand	1:3	1.5	1.03
LM	–	Lime:Metakaolin:Sand	0.75:0.25:3	–	0.94
LMO	–	Lime:Metakaolin:Sand	0.75:0.25:3	1.5	0.97

Afterwards, the specimens were stored for 23 days in a CO_2 (6%) chamber with 60 ± 10% RH at 20 ± 5 °C.

A unit of fired-clay brick was cut into prisms of ca. 50 × 50 × 30 mm, which were used to prepare plaster-brick systems by applying a layer of mortar (with a thickness of ca. 5 mm) on one of the 50 × 50 mm surfaces. The plaster used for producing the plaster-brick samples was from the same batch used for preparing the mono-plaster specimens, and they were cured at the same time and under the same conditions as described for the mono-plasters. After curing, cylindrical samples with 20 mm diameter and 35 mm in depth were cut from each plaster-brick system to perform the NMR analysis. The plaster-brick samples made of LM and LMO were not measured because the plaster layer separated from the brick during cutting.

2.2. Testing methods

2.2.1. Mercury intrusion porosimetry (MIP)

Mercury porosimetry is based on the injection of liquid mercury into a porous system by progressively increasing the pressure. At each pressure value *P*, the corresponding volume *V* of mercury contained in the cell is measured. The pressure can then be converted to an equivalent pore radius. Based on the assumption of cylindrical pores, the pore size distribution can be calculated with the Washburn equation [34]:

$$r = (-2\sigma \cos\theta)/P \quad (1)$$

where *P* is the injection pressure (Pa), *r* is the pore radius (m), θ is the contact angle between mercury and the surface (assumed to be 140° in these experiments); and σ is the interfacial tension of mercury (0.485 N/m). After substitution, we find:

$$P = 0.735/r \quad (2)$$

Eq. (2) enables deriving the cumulative injection volume from the mercury injection curve. The radius *r* is to be regarded as the size of an equivalent cylindrical pore which would fill at a given pressure. In this study, three specimens of each material were analysed with a mercury intrusion porosimeter and the pore size distributions and cumulative curves were determined. Samples of brick, mono-plaster, and plaster cured on brick were analysed; in the case of the plaster-brick specimens, the plaster layer was first separated from the brick, and plaster prismatic samples of ca. 5 × 5 × 20 mm encompassing the entire plaster thickness were prepared. Two equivalent penetrometers were used with a 5 cm^3 bulb and a total intrusion capacity of 0.500 cm^3. Low-pressure testing ranged from 6894.7 Pa to 344,737 Pa and high-pressure analysis from 275,790.3 to 172,368,925 Pa. The equilibration time was 15 s for low pressure and 30 s for high pressure.

2.2.2. Microscopy techniques (OM and SEM)

The direct observation of specimens with microscopy techniques enables examining the spatial and morphological character of porosity. Thin sections of the specimens were prepared to observe the porous structure of the plaster-brick specimens directly with the optical microscope (OM) and with the scanning electron microscope (SEM). The specimens were first dried at 60 °C and impregnated with resin under vacuum. The specimens were then polished to the thickness of approximately 20 μm and examined with OM using incident natural light. The polished sections were then sputter-coated with a thin film of conductive material (carbon) and analysed with SEM. The images were collected at an accelerating voltage of 15 kV and a working distance of 15 mm under high vacuum regime.

2.2.3. Nuclear magnetic resonance (NMR)

Nuclear magnetic resonance was used to measure non-destructively and quantitatively hydrogen atoms in the specimens, thereby getting direct information on the moisture distribution. NMR is based on the principle that in a magnetic field, nuclei have a specific resonance frequency that can be excited by a radio frequency field (42.576 MHz/T for ^1H). A specially designed NMR apparatus, operating at a field of 0.8 T, was used; its detailed description can be found in Kopinga and Pel [30] and Pel et al. [35]. A schematic representation of the probe head is given in Fig. 1. An external static magnetic field *B* is applied, and the signal from ^1H at resonance is received by the RF coil. Standard Hahn-echo techniques were used to measure the NMR signal intensity, which is proportional to the number of ^1H nuclei present. The specimens were saturated with pure water under vacuum and placed inside a Teflon holder, which has null NMR signal and has only one open side from which the sample can dry (one-dimensional drying). A standard (solution of $CuCl_2$) placed at the bottom of the holder was also measured to monitor the sta-

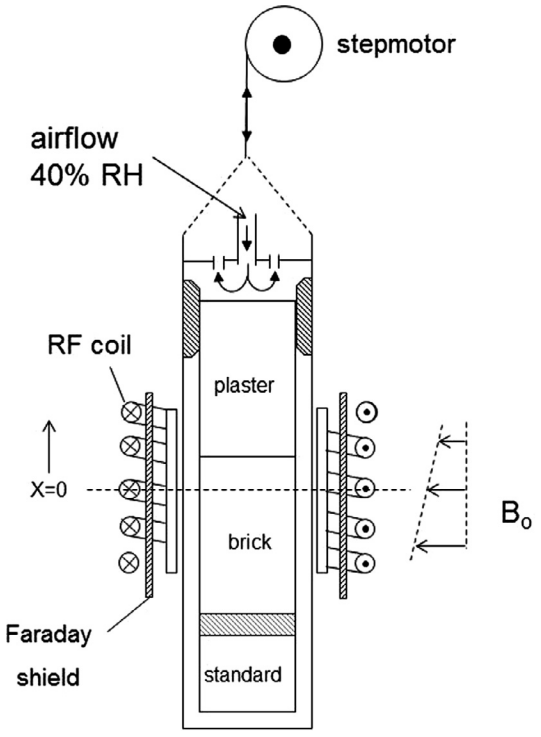

Fig. 1. NMR apparatus for measuring the moisture profiles during the drying experiments.

bility of the apparatus. The samples were moved in the vertical direction (along *x*) using a step motor to make measurements at different positions, so a complete moisture profile was obtained. The magnetic field gradient was chosen so that a slice of less than 2 mm could be measured. Continuous airflow with a RH of 40 ± 5% at 20 ± 2 °C temperature was blown over the sample at a flow rate of 2 $L{\cdot}min^{-1}$. Measuring one moisture profile takes about 20 min. The complete drying experiment takes an extended period (1 – 2 days), so small variations in the moisture profiles during a single scan can be neglected [36].

NMR can also give additional information by simultaneously measuring the relaxation time of the water inside the pores of a material, i.e. the relaxation time can provide information on the pore size distribution [31,37]. In this study, we have measured the so-called spin-spin relaxation time, and the following equation shows that the relaxation time is proportional to the surface-to-volume ratio of a pore [31]:

$$1/T_2 = \rho_2(S/V) \quad (3)$$

where T_2 is the transverse relaxation time, resulting from surface interactions, ρ_2 is the surface relaxation strength. In the case of a spherical pore, this can be simplified to

$$T_2 = 3r/\rho_2 \quad (4)$$

where the relaxation time is proportional to the pore size and enables the determination of the 'pore water distribution' in a material, i.e. the distribution of the pores filled with water.

3. Results and discussion

3.1. MIP and microscopic observations

The physical properties of the materials determined with MIP and the amount of water absorbed by saturation under vacuum before performing the NMR experiment are given in Fig. 2, and the pore size distribution curves are presented in Fig. 3. The vacuum saturation condition is not representative of what occurs in natural exposure conditions, but it was used because it was also the aim of the experiment to determine the pore water distribution during drying by measuring the transverse relaxation time (T_2). The porosity increases significantly in LO (ca. 10%) when the plaster is applied and cured on brick, whereas the slight increment registered in L (ca. 3%) is within the error margin. The different methods used in the preparation of the two types of specimen (mono-plaster and plaster on brick) can influence the microstructure of the materials; the two mortar compaction methods and the vibration introduced during cutting of the hardened plaster-brick specimens. The compaction method used for the plaster-brick preparation could be less effective in eliminating the entrained air observed further in LO. The cutting vibration could originate microcracks. Also, the different specimen geometry (mono-plaster and plaster-brick) can influence the hardening reactions, which also affects the microstructural properties. The substitution of a part of lime by metakaolin does not seem to affect the porosity, but the addition of oil to LM induces an important increment. This phenomenon is further discussed along with the observations under the OM.

Figs. 4 and 5 show representative OM views of the thin sections of mono-plaster and plaster-brick specimens, respectively. Plaster L exhibits a severely cracked matrix (crack widths ranging from 10 to 50 μm) affecting the groundmass and the ITZ. Plaster-brick LB shows fewer cracks, which have widths far lower than the ones observed in the mono-plaster (ranging from 10 to 17 μm). Plaster LO and plaster-brick LOB show a much less cracked matrix than L specimens, and exhibit rounded large pores with diameters ranging from 20 to 60 μm.

Mono-plasters of LM and LMO show a dense structure, indicating that the addition of metakaolin inhibits the formation of shrinkage cracks. Sample LMO also shows large rounded pores. The round-shaped pores present in the mixes with oil can be attributed to entrained air during the mixing process, because vegetable oils can act as air entraining agents [38]. They are mainly composed of glycerides, which are not chemically stable in the alkaline interior of lime mortar, consequently hydrolysing to glycerol and fatty acid anions, the latter consisting of non-polar hydrocarbon chains (hydrophobic units) linked with polar hydrophilic carboxyl groups ($-COO^-$) [39]. On the gaseous and liquid phase interface, the polar groups are directed to water and they lower

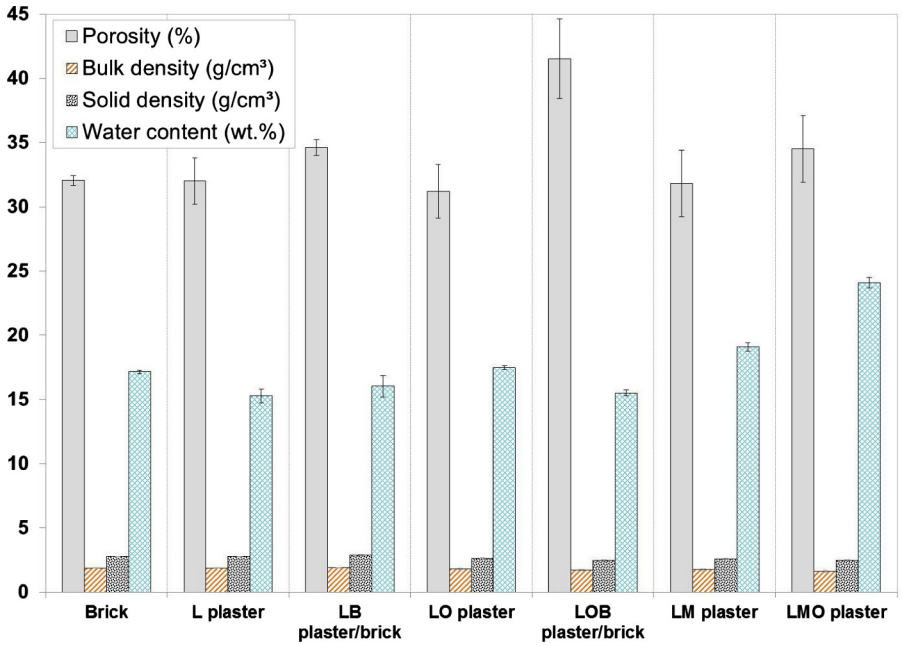

Fig. 2. Values of porosity and density obtained with MIP, and water content of the samples before the NMR analysis (average of three measurements).

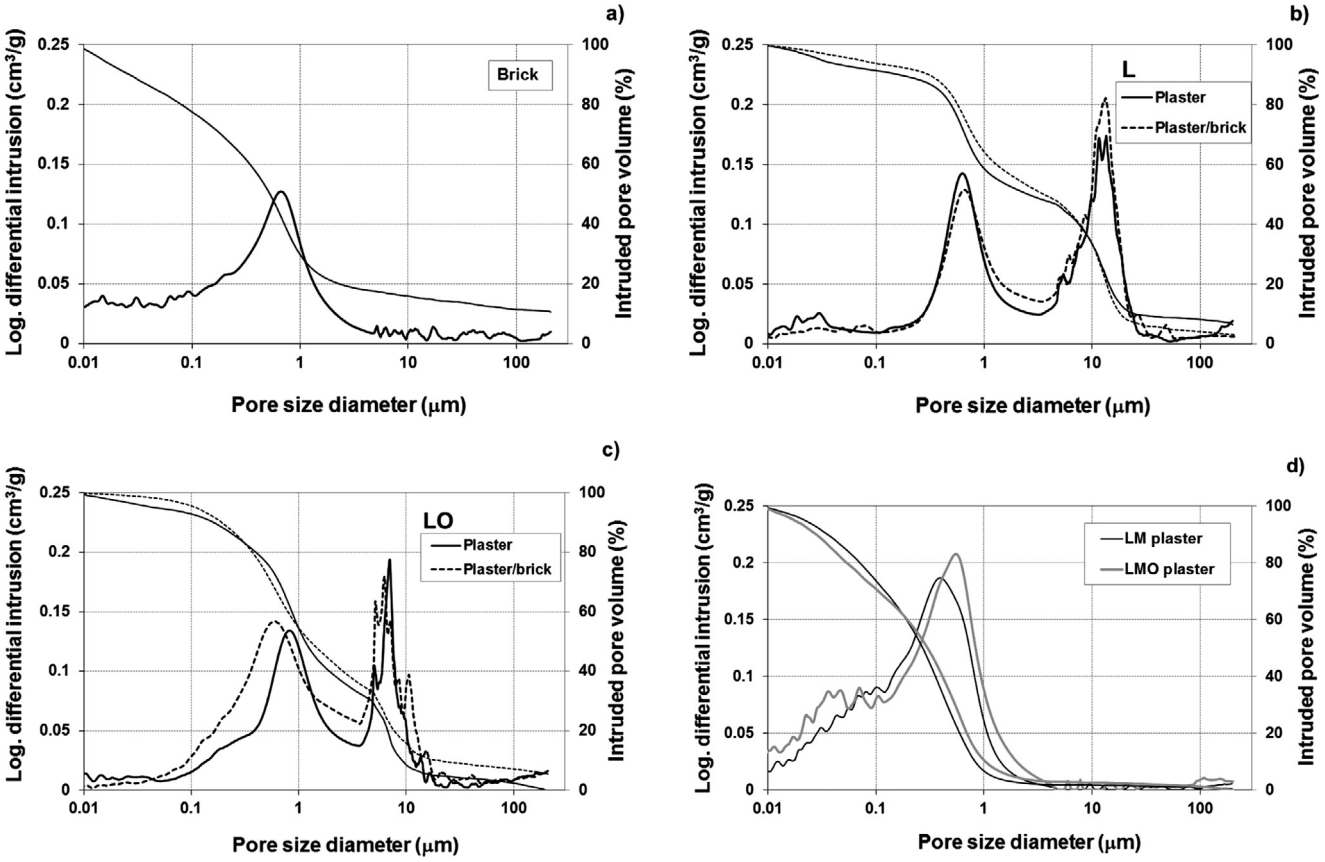

Fig. 3. Pore size distribution obtained with MIP of brick, plaster, and plaster-brick specimens.

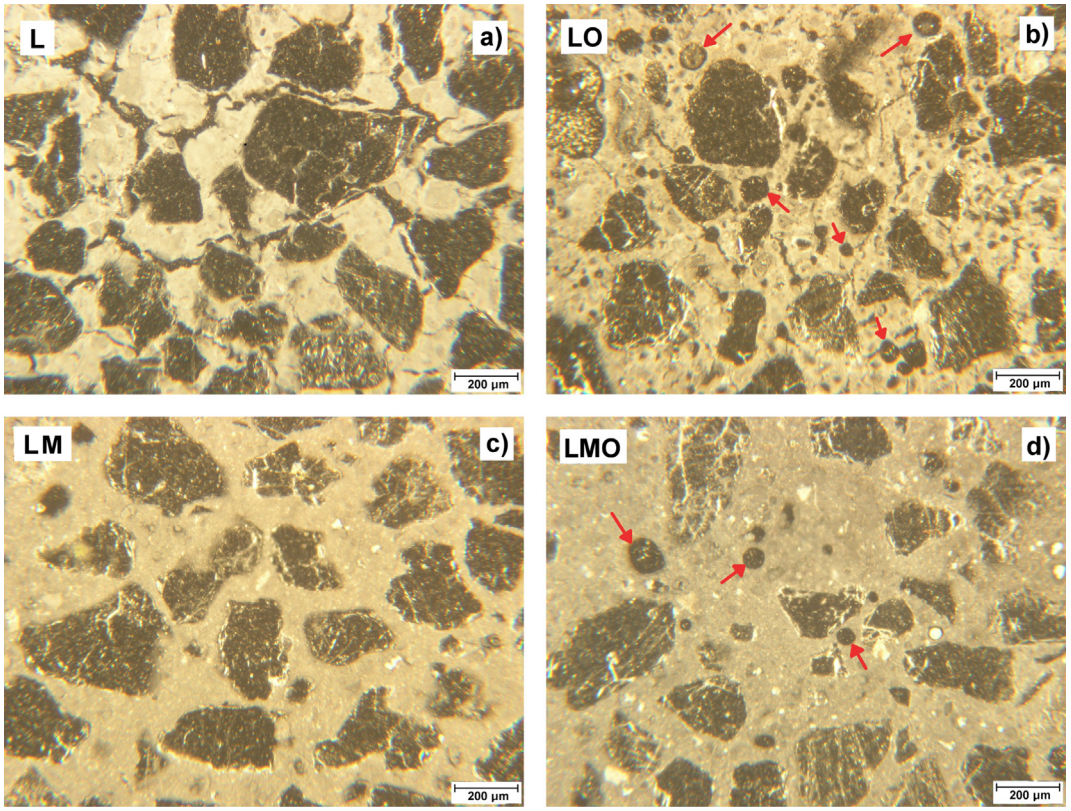

Fig. 4. Thin section photomicrographs of the mono-plasters; some of the largest rounded pores observed in the mortars with oil are highlighted with a red arrow

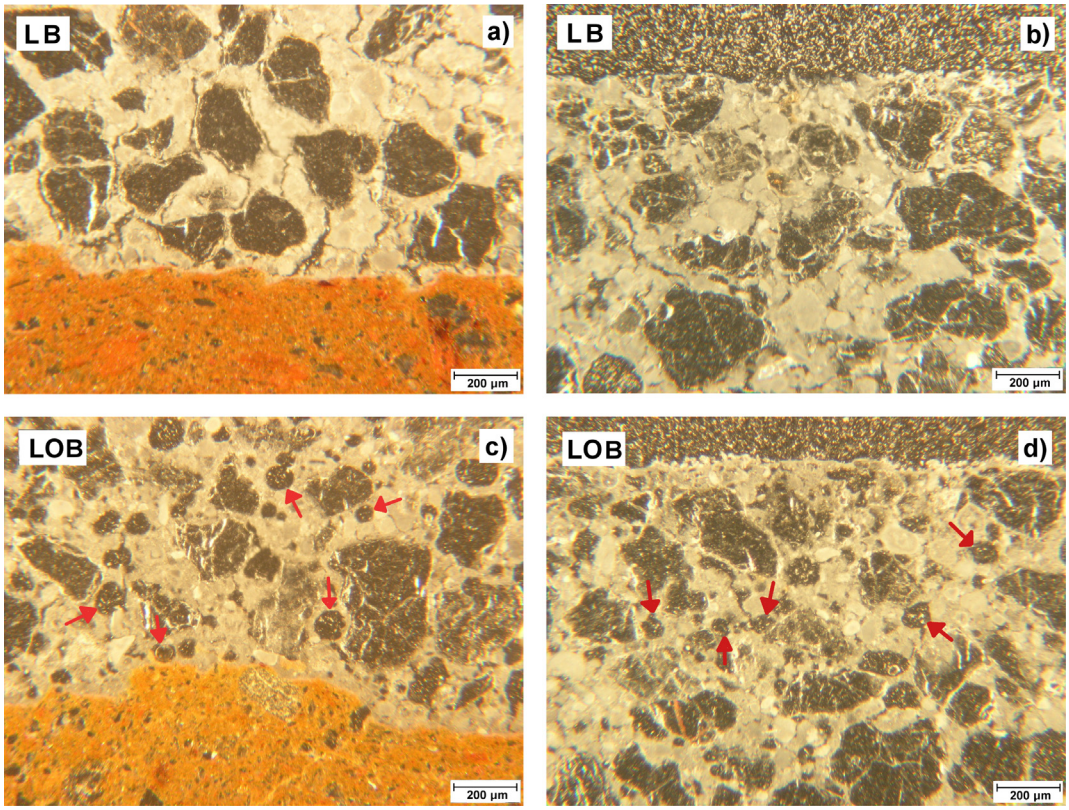

Fig. 5. Thin section photomicrographs of the plaster-brick systems: a, c) view of the plaster-brick interface; b, d) view of the top of the plaster; some of the largest rounded pores observed in the mortars with oil are highlighted with a red arrow. (For interpretation of the references to colour in this figure legend, the reader is referred to the web version of this article.)

its surface tension, thus facilitating the formation of air bubbles [38]. The carboxyl groups will coordinate with calcium, and the non-polar "tails" will be directed to the air-interface, thus imparting water repellency.

The observation of the thin sections confirm the MIP results of the lime mono-plaster and plaster-brick specimens regarding the significant volume of pores showing up within the macropore region (around 10 µm). In the case of mono-plasters L and LO, the macropores seem to be mostly assigned to cracks, which are considerably wider in L. Plaster LO shows large pores with rounded shape, some of which interconnected by narrower cracks; the MIP distribution curves also show that the pores in the macropore region were slightly shifted to lower pore sizes when oil was added to lime. The thin section of LMO mono-plaster indicates that the high porosity value obtained with MIP can be attributed to the rounded pores developed. However, the macropores larger than 30 µm observed in the thin sections of LMO, and also of LO, were not detected with MIP. This can be attributable to the ink-bottle effect [40], or to the fact that some of the pores are isolated and hence not intrudable by mercury [25], or because the high-pressure intrusion by mercury may reduce the number of large pores due to the shielding effect of smaller pores [41]. The fact that the increment in porosity assigned to oil addition was detected by MIP in LMO, but not in LO can be attributed to the different structure of the specimens combined with the MIP limitations.

Fig.6 gives backscattered electron images of the plaster-brick samples. The higher porosity of LOB in comparison to LB is confirmed by the photomicrographs, which show large rounded pores within the mortar matrix. Sample LB also shows air entrained pores (rounded), but of considerably lower size.

The elemental composition of the plaster-brick specimens was analysed with SEM-Energy Dispersive X-ray Spectroscopy (SEM-EDX) to investigate the occurrence of pozzolanic reactions across the plaster-brick interface by observing the distribution of Si, Al, and Ca [42]. Fig. 7 shows the microstructure and elemental composition of LB plaster-brick interface. The SEM photomicrographs and elemental maps did not reveal any reaction rim neither aluminum nor silicon enrichment across the interface area as a result of hydraulic reactions between the both components. Hence, we could not prove the occurrence of pozzolanic reactions across the plaster-brick interface.

The results obtained with MIP, OM, and SEM indicate that the addition of oil can hinder crack formation assigned to drying shrinkage, possibly thanks to the development of large rounded pores, because shrinkage is increased when porosity is decreased (large air entrained pores do not contribute to shrinkage); this is explained by the fact that crystallinity is also decreased [43]. The substitution of a part of lime by metakaolin also contributes to the reduction of shrinkage cracks and promotes a good bond in the ITZ. The porous structure of L and LO mono-plasters changes when they are applied and cured on brick. As previously mentioned, the different specimen preparation methods are likely to influence the microstructure of the plasters. Moreover, although not proven in this study, pozzolanic reactions may occur at the plaster-brick interface. These features will influence the drying behaviour of the materials as discussed in the next section.

3.2. Moisture profile measurements during drying by NMR

3.2.1. Drying of mono-material samples

The first measurements were focused on the drying behaviour of brick and mono-plaster samples. The NMR moisture profiles

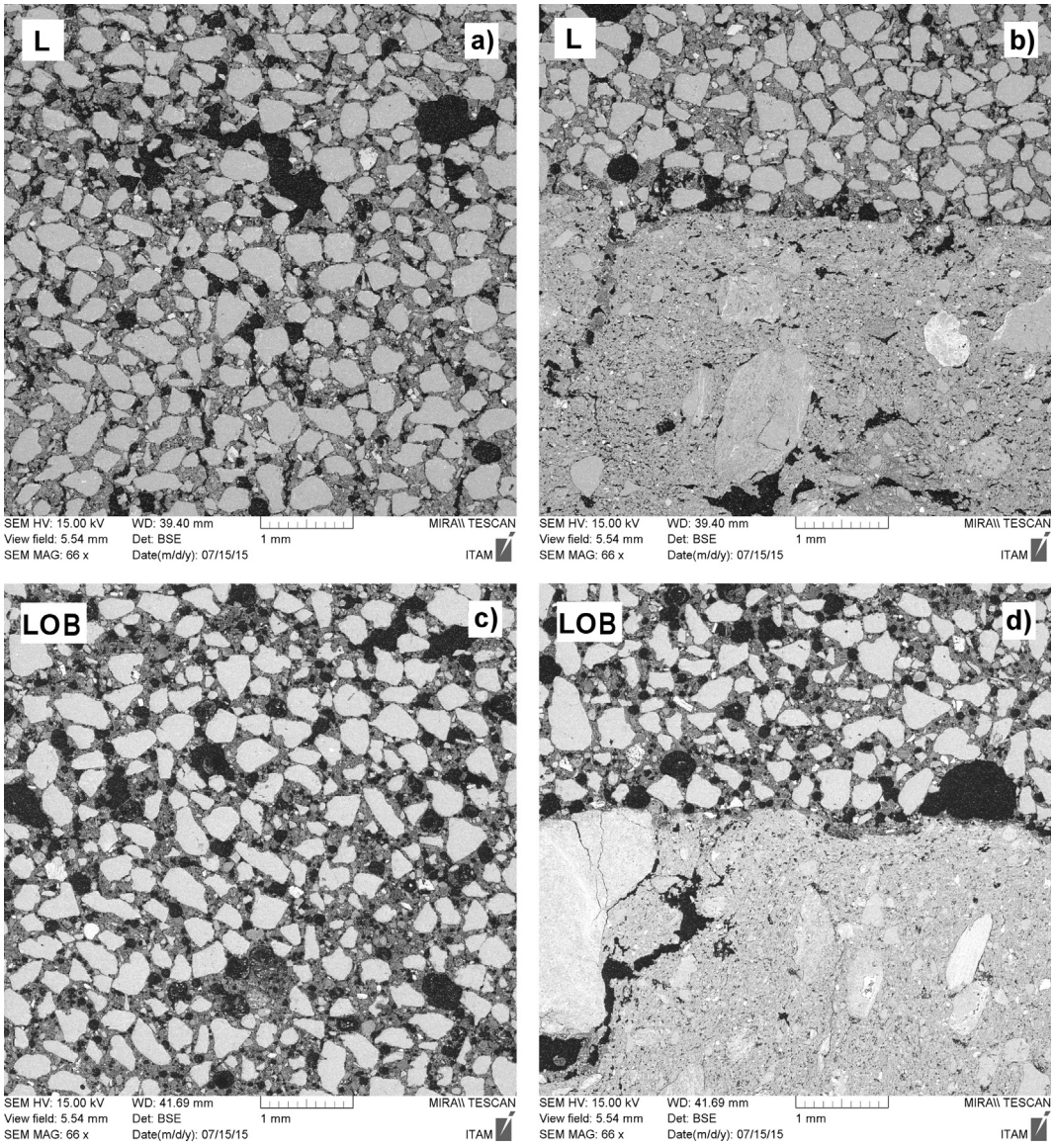

Fig. 6. SEM photomicrographs of the plaster-brick specimens: a, c) view of the plaster matrix at the middle of the layer; b, d) view of the plaster-brick interface.

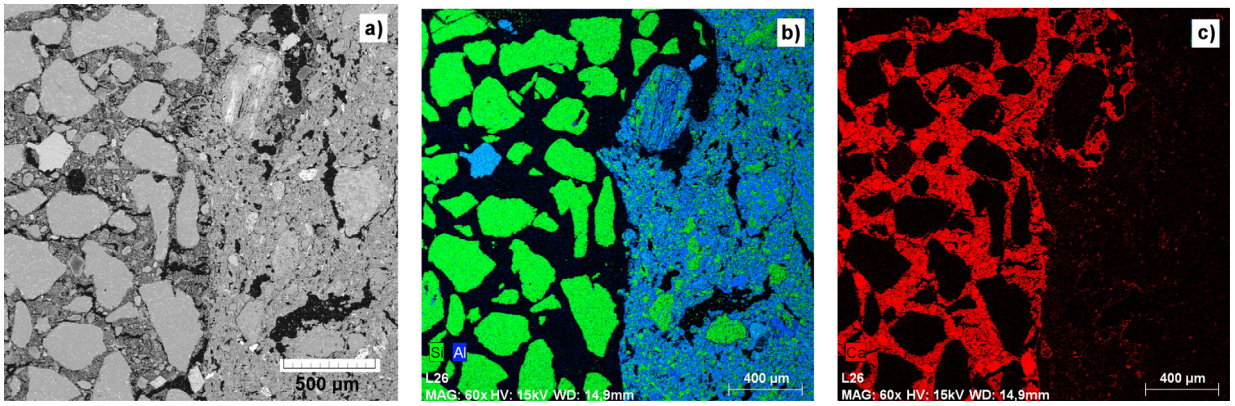

Fig. 7. BSE image and SEM-EDX elemental maps: a) Interface between plaster (left) and brick (right); b) Si (green) and Al (blue) across the interface; c) Ca (red) distribution across the interface. (For interpretation of the references to colour in this figure legend, the reader is referred to the web version of this article.)

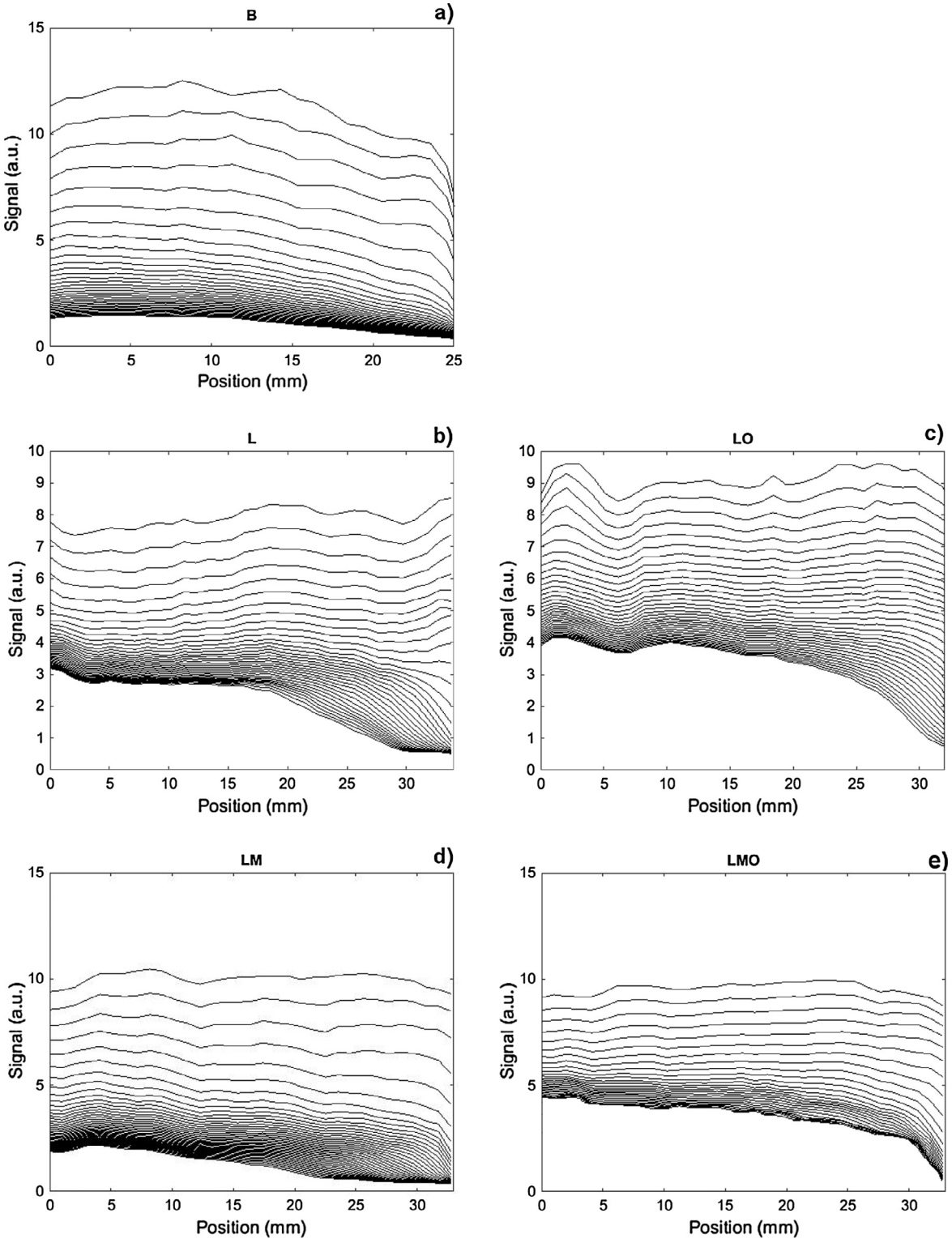

Fig. 8. NMR moisture profiles during drying of brick and mono-plaster specimens. The time between subsequent profiles is 1 h, and the profiles are given for a total period of 38 h (the drying surface is always on the right).

during drying are given in Fig. 8. The profiles of all specimens show some variations that are substantially larger than the experimental noise and reproduce from profile to profile. These variations reflect inhomogeneities in the specimens as reasoned by Pel et al. [44]. Fig. 9 shows the drying curves of the materials, i.e. the moisture content as a function of time, at position 5 mm (ca. 20–25 mm from the exposed surface) and at ca. 3 mm from the surface.

At high levels of moisture content, the moisture migration is dominated by liquid transport; the almost horizontal profiles reveal high moisture diffusivity. As the moisture content decreases, the large pores are drained and will no longer contribute to liquid

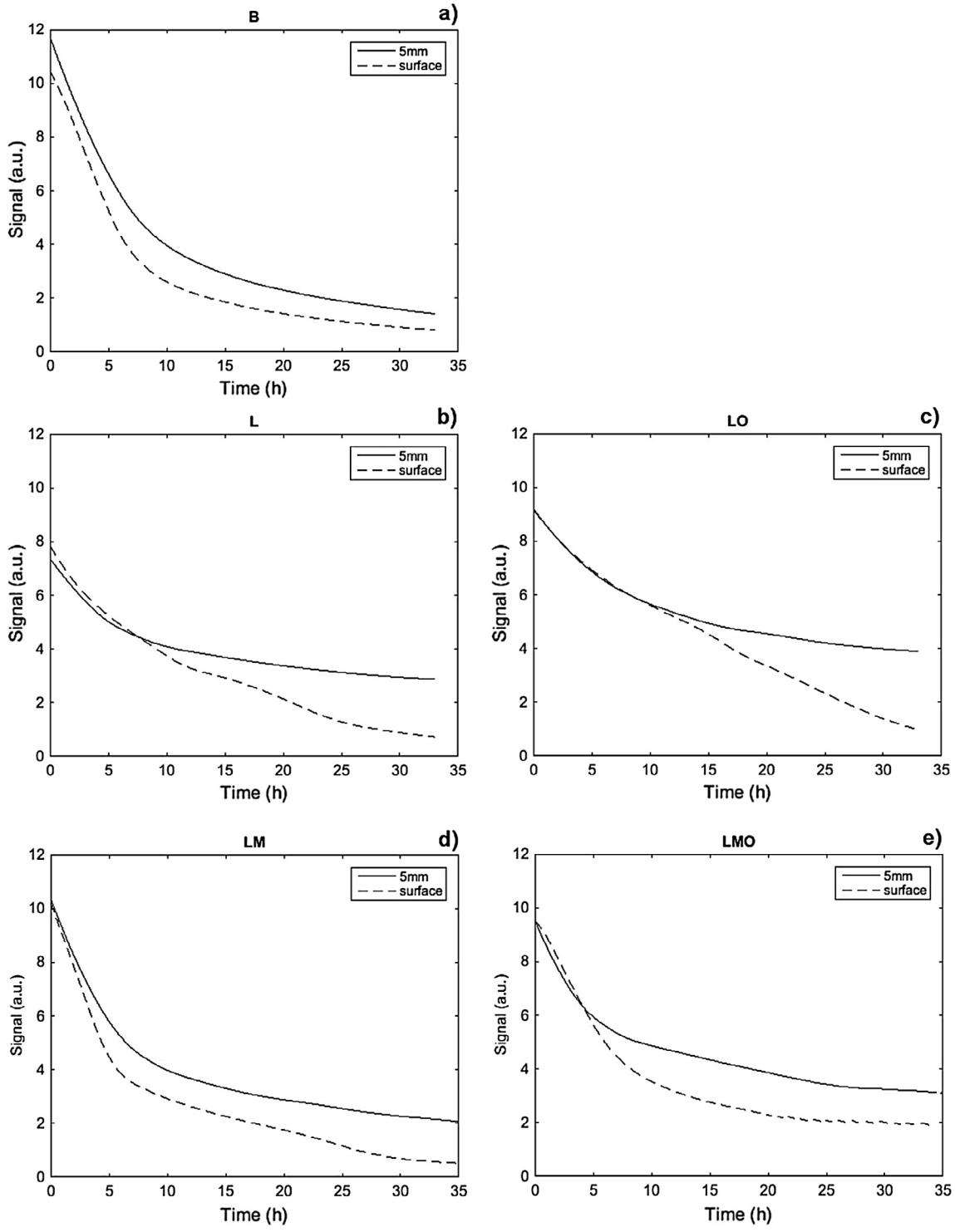

Fig. 9. NMR drying curves of brick and mono-plasters measured at position 5 mm (distance from the evaporating surface) and at ca. 3 mm from the exposed surface.

transport; the moisture diffusivity decreases. The vapour pressure will then govern the moisture migration. The transition from liquid transport to vapour transport corresponds to the drying front observed in the moisture profiles [44–46]. As soon as drying has started, heat is extracted and the temperature at the top of the sample decreases. When the receding drying front penetrates the material, drying is internally limited by vapour transport and, hence, the drying rate and the heat extracted from the sample is strongly reduced. After a certain period, the experiment can be regarded as isothermal [45,46].

The brick moisture profiles indicate that the moisture diffusivity throughout the drying process is very high in this material, as the profiles remain relatively flat throughout the entire experiment, and only a very smooth drying front develops. As mentioned, as long as some continuous liquid network exists in the porous structure, drying mainly results from liquid transport (unsaturated capillary flow) [47]. Keita et al. [48] claim that interpreting only the

water mass loss as a function of time may lead to erroneous conclusions. The authors have recently shown experimentally and with 2D finite element method, that as desaturation proceeds, the drying rate is reduced even if the capillary flow still supplies water to the surface. As the wetting surface at the entrance of the capillaries decreases, the drying rate decreases even if no receding front progresses. According to the mentioned arguments, the moisture profiles of the brick indicate that the capillary effects are dominant in the evaporation process, i.e. the evaporation is effectively supplied by capillary induced flow from large pores at the receding front feeding fine pores at the evaporating surface. As a result, the drying front is very smooth.

Figs. 8 and 9 show that the reference plasters dry faster than the plasters with oil. Shahidzadeh-Bonn et al. [17] study on the effect of wetting properties on the kinetics of drying of porous media showed a considerable suppression of evaporative water losses from hydrophobic porous media relative to hydrophilic media. The evaporation suppression in hydrophobic media being attributable to the interruption of capillary liquid flow and reduction in capillary driving force. In the case of LO and LMO, the drying rate is not much altered with respect to L and LM, respectively. Thus, one can assume that LO and LMO plasters have a certain amount of pores that are not lined with nonpolar molecules and allow effective liquid transport by capillarity. On the other hand, the degree of wettability also influences liquid transport and the large rounded pores observed in LO and LMO plasters can counteract the water-repellent effect. Given that the water vapour diffusion of the plasters with oil is also similar to the references, as determined in a previous study [49], the global drying kinetics are not much altered with respect to the references.

A non-zero residual moisture content is observed at the end of the experiment in all plasters. Plasters with oil show higher moisture content at the end of the experiment; ca. 3 wt% for L and LM, and 5 wt% for LO and LMO, measured gravimetrically. The contact angle between water and the material, which was not measured in this study and is probably higher in the case of mortars with oil, can influence the residual moisture content. Moreover, LO and LMO were the materials that absorbed the highest amount of water under vacuum saturation (Fig. 2) and, given that they dry slower than the reference plasters, it is natural that they have higher water content after the same drying period.

Fig. 9 shows that the drying rate during stage I is analogous in all materials in both the layers located deep inside the samples and close to the surface, except in the case of LM where initially, the drying rate is slightly faster at the surface. During stage II, drying in the deeper layers of the materials becomes constant at a considerably high moisture content level, whereas close to the surface the materials reach an almost zero moisture content, except in LMO. These results indicate that the deeper layers of the materials are not drained, probably due to the interruption of the capillary liquid flow combined with the increment in the flow path. As a result, a considerable part of the water that was introduced into the system remains trapped in the deeper layers of the materials.

3.2.2. Drying of plaster-brick systems

The drying moisture profiles of plaster-brick systems are given in Figs 10 and 11 shows the drying curves of the materials for an easier comparison between the two systems. The drying curves are given at position 5 mm and 32 mm (ca. 3 mm from the exposed surface); position 5 mm corresponds to brick and position 32 mm corresponds to plaster. The moisture profiles show a significant dip in the signal intensity at the plaster-brick interface, which is probably related to variations in porosity and composition. The change in porosity in LB near the plaster-brick transition zone can be attributed to the water flow from the fresh plaster to the brick during the bonding process; during the initial bonding, small binder particles can be transported towards the plaster-brick interface and the plaster becomes more compact (enriched in binder) at the interface [50]. Brocken [19,22] has studied the phenomenon of water suction from a cement plaster to brick and reported that the water retentivity of the plaster, i.e. the amount of water withhold by the fresh plaster, is decreased by the addition of an air-entraining agent. Linseed oil also acts as an air entraining, therefore, the water retentivity of LOB plaster could be lower than that of LB, resulting in better water extraction from the plaster to the brick and consequently contributing to a better particle packing at the interface. However, LOB shows a significantly lower dip in moisture content at the interface, indicating lower bond strength. The poor bond strength of air entrained mortars to substrates can be attributed to the myriad of microscopic and macroscopic air bubbles at the bond plane [51]. Another factor that can account for lower bond strength between the plaster with oil and the brick is the mismatch between the surface energy of both materials, i.e. partially hydrophobic plaster vs hydrophilic brick. The plaster-brick interfaces in Fig. 10 are represented by a grey area, the width of which is clearly larger in LB in comparison with LOB and can result from the better interpenetration of both layers' porous structures. It could also be influenced by the flatness and

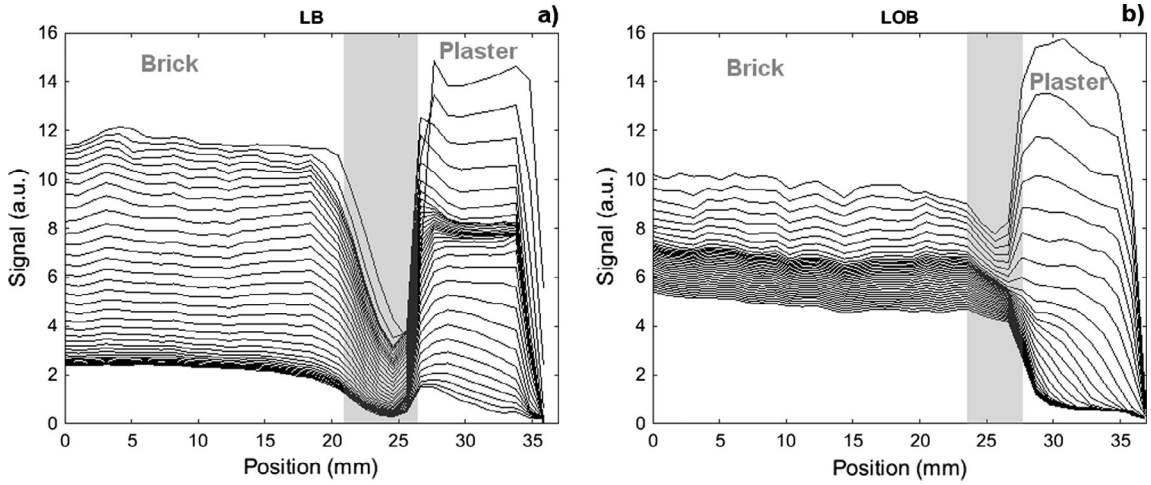

Fig. 10. NMR moisture profiles during drying of plaster-brick systems: a) lime; b) lime with oil. The time between subsequent profiles is 1 h, and the profiles are given for a total period of 38 h (the drying surface is always on the right, i.e. the plaster surface). The interface is represented by the grey area.

perpendicularity of the plaster-brick interface in relation to the axis of the cylindrical specimen.

The moisture content decreases at a faster rate in the plaster layers than in the brick. This indicates that the capillary suction of the pores in the plasters is higher than the capillary suction of the pores in the brick. In the case of LB, the residual moisture content in the brick at the end of the experiment is analogous to the drying of the brick mono-material sample (Figs. 8a and 9a). The moisture profiles are relatively flat for both plaster and brick, suggesting that capillary flow is the dominant transport process.

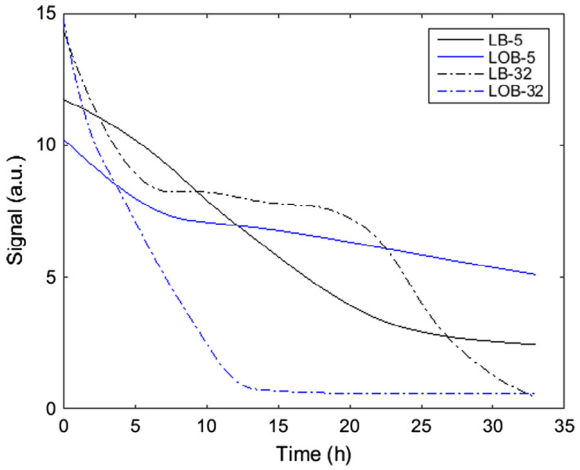

Fig. 11. NMR drying curves of plaster-brick systems at position 5 mm and at position 32 mm.

Initially, drying is faster in LOB system, as revealed by the higher reduction in signal intensity between profiles and by the slope of the drying curves. This can arise from the significantly higher porosity of LOB plaster with respect to LB and from the higher interconnectivity between pores (Fig. 2) resulting in effective capillary drainage of the large pores at the initial stage, even though a part of the porosity may not allow liquid transport. However, although initially, the brick dries at a slightly faster rate compared with LB, after 8 h the drying rate becomes extremely slow while the plaster layer continues drying and reaches an almost zero residual moisture content after 17 h. The residual moisture content in the brick at the end of the experiment is significantly higher than that of the individual brick specimen. As mentioned, as the plaster layer becomes unsaturated, air first replaces some of the water in the larger pores, subsequently causing the water to flow through the smaller pores with an increased tortuosity (and hydrophobic constriction) and an increase in the flow path. This leads to a resistance for water to flow from the brick to the plaster when the air/water interface reaches the brick where, as mentioned earlier, the capillary effects are dominant in the drying process. The large rounded pores and lower bond strength at the interface between the plaster and the brick in LOB can play a major role in creating an hydraulic resistivity to liquid moisture transport because when the interface voids reach a certain unsaturated state,

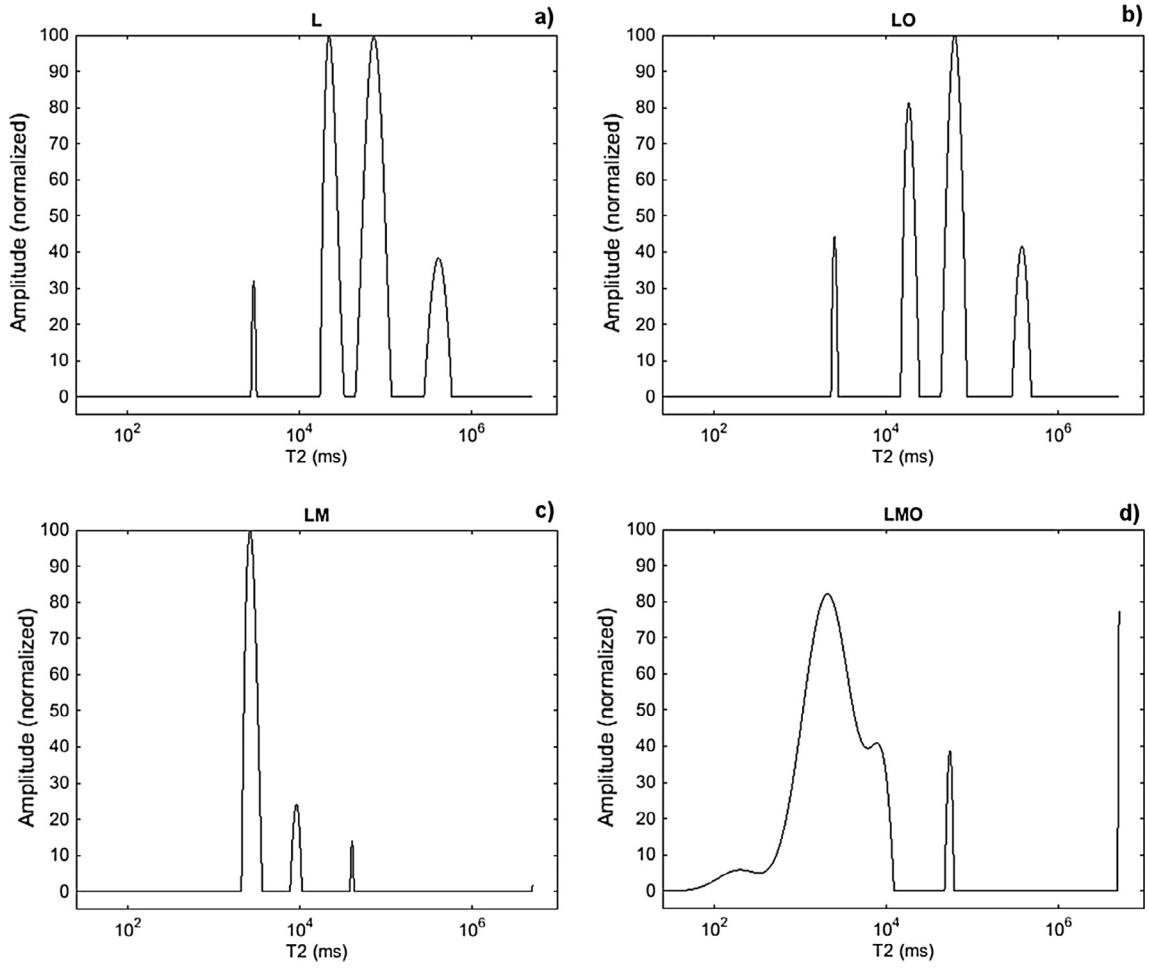

Fig. 12. Pore water distribution of water saturated L and LO mono-plasters determined by NMR-T2 relaxation.

fluid transport is no longer possible between the brick and the plaster. From this period onwards, the moisture transport from the brick to the plaster can only occur by diffusion; liquid water flows up to the hydrophobic/hydrophilic interface, vapourises and diffuses through the hydrophobic dried layer resulting in a constant diffusive flux. As mentioned, the mismatch between the physical-chemical properties of the different systems (brick and plaster), namely the different pore network and surface energy, can contribute to enhance the hydraulic resistivity by affecting the bonding process. As discussed by Freitas et al. [52], the interface between layers can lead to a hydric resistance (due to the interface itself) resulting in a faster drying of the outside layer due to restrictions in the supply of water and a slowing of the drying of the inside layer. The results obtained are also in line with those reported by Gonçalves et al. [14] and Shokri et al. [53], who investigated the drying behaviour of a water-repellent lime-based plaster applied on stone, and the liquid phase continuity and drying of a column composed of a thin hydrophobic layer of sand over a hydrophilic layer, respectively. In both cases, the authors discussed that the presence of a water-repellent layer resulted in the reduction of cumulative evaporation and formation of a stationary vapourisation plane. The authors attributed these changes to the interruption of hydraulic connectivity between the receding the drying front and the evaporating surface, and to alteration in contact line motions.

In contrast, Kim et al. [54] recent study with hydrophilic and hydrophobic sands of different grain sizes showed that the evaporation process depends strongly on the pore size distribution. In their study, at the early stage of drying, both wettable and water-repellent sands exhibited the same evaporation rate, which is dominated by boundary conditions and capillary effects. Later, the water-repellent sand showed faster drying rate than the wettable sand. Moreover, the water-repellent sand facilitated the evaporation when both hydrophilic and hydrophobic sands were in contact. Their experimental observations suggested that the surface wettability may not be a sole factor influencing the drying process while the degree of hydrophobicity, particle size distribution and initial wetting condition are predominant when assessing drying mechanisms. The authors claim that once the drying front reaches a certain critical depth, the effects of pore size distribution and surface tension can be interblended.

Wu et al. [55] recently developed a 3D pore network model to study the drying process in various hydrophobic porous media. The influence of the pore size distribution and the throat-to-pore ratio were in focus. The authors concluded that the evaporation process in the hydrophobic network of the high throat-to-pore ratio was similar to that in the hydrophilic network. As compared to the hydrophobic narrow pore size distribution network with a high throat-to-pore ratio, the reduction of the drying rate at the initial stage was smaller, and the constant evaporation rate period was shorter in the case of the wide pore size distribution. This indicates that the type of network significantly affects the characteristics of each drying stage in both hydrophobic and hydrophilic porous media. The study by Wu et al. accounts in explaining the

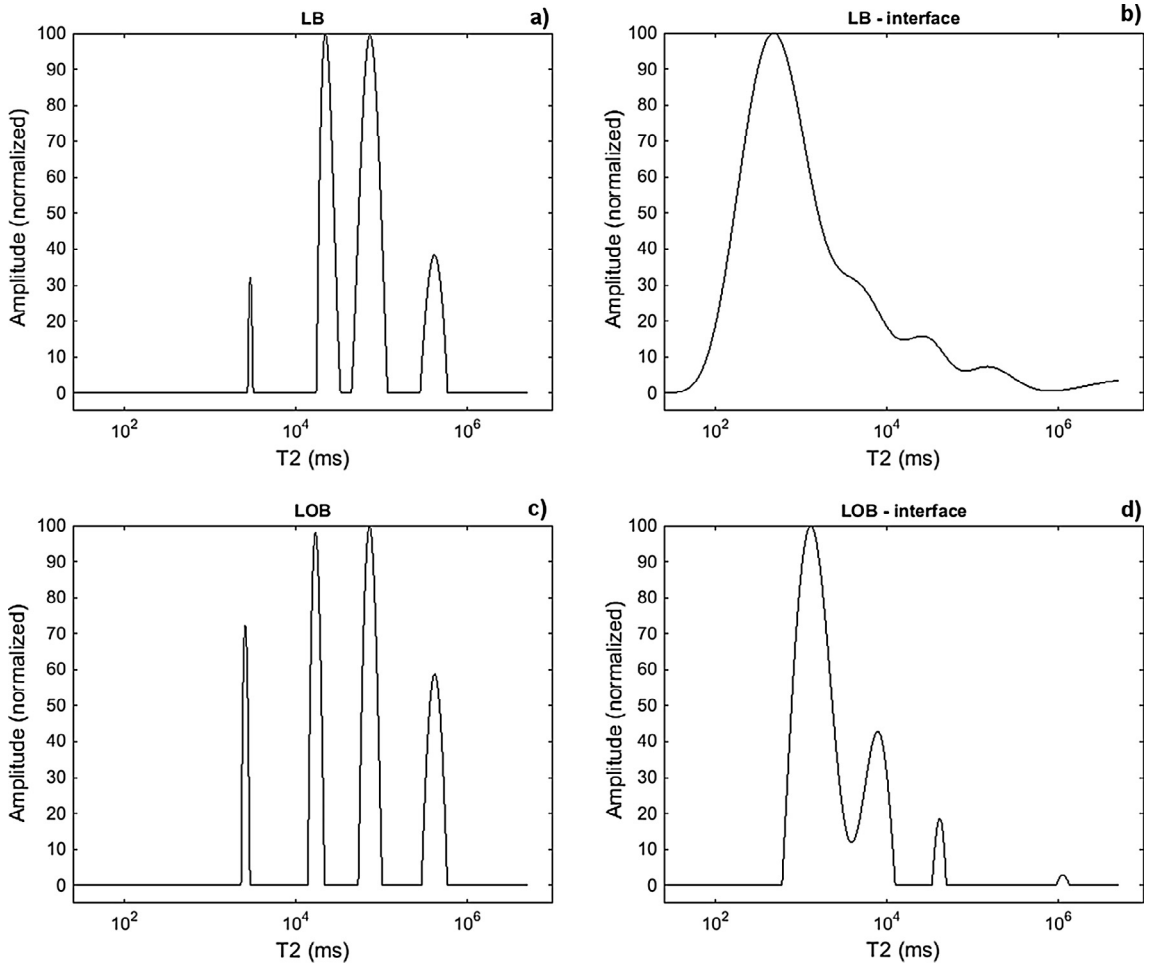

Fig.13. Pore water distribution of plaster-brick systems determined by NMR-T_2 relaxation: a) Middle of the lime plaster; b) Interface between the lime plaster and brick; c) Middle of the lime with oil plaster; d) Interface between lime with oil plaster and brick.

different drying behaviour obtained between the different types of specimens prepared, i.e. mono-plaster vs plaster-brick samples. Varying the binder composition, water:binder ratio, and combination with a porous substrate influences significantly the porosity and pore network of both hydrophilic and hydrophobic materials, which is in turn reflected in the drying kinetics.

3.2.3. Pore water distribution

As mentioned earlier, in NMR relaxation a T_2 distribution is similar to a pore size distribution, where each relaxation time corresponds to a pore size filled with water. According to Eq. (1), the smallest pores have the shortest relaxation times, and the largest pores have the longest relaxation times. Figs. 12 and 13 show the T_2 spectra distribution of water saturated mono-plasters, and of LB and LOB plaster-brick specimens, respectively.

For L and LO mono-plasters the MIP results revealed that both samples have a bimodal distribution with ca. 60% of the pores centred around 1 μm diameter and ca. 30% of the pores centred at around 10 μm. The NMR-T_2 distribution detected four types of pores as shown by the four peaks in the T_2 distribution. It is reasonable to infer that the largest macropores, including those that were not detected by MIP, are represented by the relaxation peak with the highest relaxation time. Mono-plaster LM shows a trimodal distribution with lower relaxation times than the lime mono-plasters, which is in line with the MIP and OM observations. Mono-plaster LMO shows a broad distribution between 10^2 and 10^4 ms, which can indicate the existence of interconnection between different types of pores that were not detected or distinguished with MIP.

Mono-plasters L and LO, and plasters LB and LOB show a similar tetramodal T_2 distribution, with the third peak having the highest amplitude. As mentioned, the fourth peak, with the largest relaxation time, can represent the largest pores; its amplitude is higher in LOB and may correspond to the largest rounded pores observed with OM. The first peak, with the shortest relaxation time, could be assigned to water in pores below 1 μm; its amplitude is also higher in LOB, which is in line with the MIP results that show a higher volume of pores in this region. Fig. 13 also gives the T_2 spectra measured at the interface between plaster and brick. The T_2 distribution confirms that the plasters have smaller pores at the interface since the relaxation times are shorter ($<10^4$ ms). Plaster LB has smaller pores across the interface than LOB, which is in line with the OM and SEM observations. The existence of smaller pores at the interface explains the dip in the signal intensity observed in the moisture profiles of LB plaster (Fig. 10.a). The broad distribution of LB can represent multiple interconnected pore types. Plaster LOB interface is also characterised by smaller pores than at the middle of the plaster thickness, but the T_2 distribution indicates that the connectivity between the pores is much lower than in LB; only the two first pore types (corresponding to the two first peaks) seem to be connected. This is in contradiction with the MIP results discussed in Section 3.1 (Fig. 2). However, the MIP results regard the entire sample thickness, and the properties of the plaster vary as a function of distance to the brick-plaster interface, which NMR can detect. Moreover, LOB shows two peaks of low amplitude above 10^4 ms, which could correspond to the large rounded pores observed with SEM. However, the magnitude of

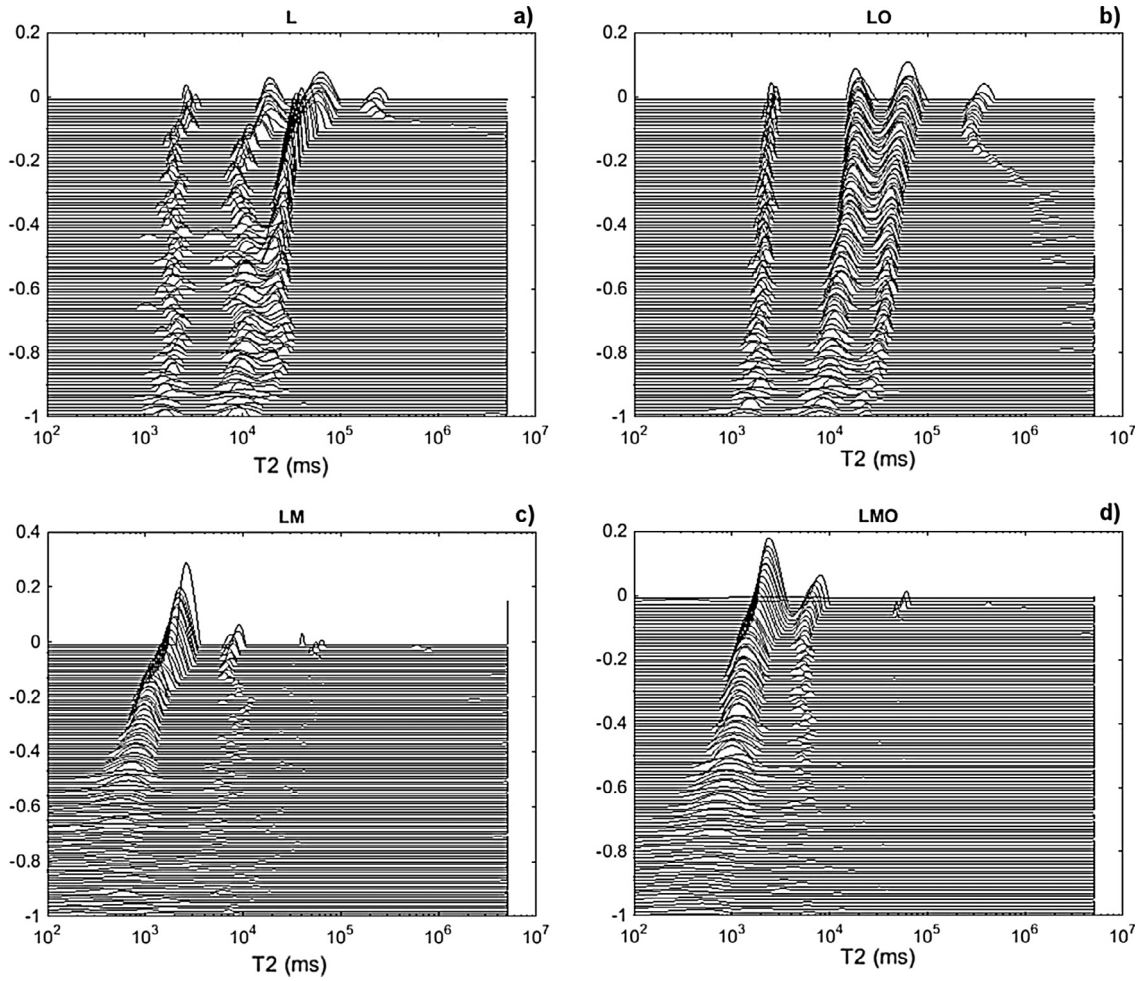

Fig. 14. Pore water distributions in the middle of the mono-plaster samples for 20 min steps as determined from T_2 relaxation measurements during drying.

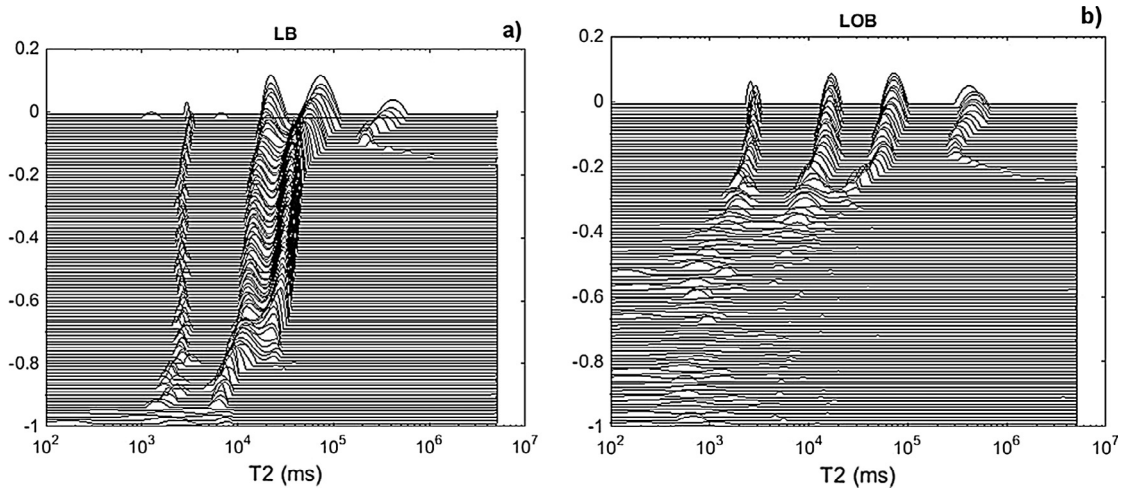

Fig. 15. Pore water distributions in the middle of the plaster layer of the plaster-brick samples for 20 min steps as determined from T_2 relaxation measurements during drying.

these pores was expected to be higher, as indicated by the amount of large rounded pores observed with SEM at the interface. Some of the pores in LO can correspond to isolated pores, which remained empty after the vacuum saturation. Hence, these pores cannot appear in the T_2 distribution.

Figs. 14 and 15 show the pore water distribution in the mono-plaster and plaster samples, respectively, as a function of time during drying for a total period of 32 h. It can be seen that the pores with the largest relaxation times are more rapidly drained, whereas the pores with lower relaxation times dry much slower and are not completely emptied at the end of the experiment. The pores in mono-plasters LM and LMO are drained at a faster rate compared with L and LO, indicating that the capillary flow is more efficient in these materials. The pores in plaster LOB are rapidly emptied during the 17 h period, as mentioned earlier, whereas the pores in plaster LB remain saturated almost until the end of the experiment, reflecting the capillary flow from the brick to the plaster layer.

4. Conclusions

In this study, NMR was used to investigate the drying process of lime-based plasters and plaster-brick systems, and to examine the pore types by measuring the number and position of T_2 spectra distributions. The T_2 spectra could be well correlated with the results obtained with MIP and SEM; MIP gave information about the pore size entrances, SEM showed the pore spatial distribution and NMR-T_2 relaxation provided information about the pore water distribution at different distances from the plaster-brick interface. The NMR-T_2 results indicated that pores with the same entrance size encompass different pore size geometries. Besides distinguishing different pore size geometries, the NMR relaxation technique enables the analysis of the specimen at a precise position, which is extremely advantageous when studying layered materials.

The NMR moisture profiles showed that lime with oil plaster inhibited the drying of the brick where it was applied. Given that the mono-material plaster samples (mono-plasters) showed similar drying kinetics between L and LO, the main reason for the remarkable decrease in the drying rate of the lime with oil plaster-brick system seems to be mainly related to an hydraulic resistivity created at the interface between the plaster and the brick. Thus, the combination of mortars with substrates is of great importance in the study of the drying kinetics of a layered system. When a plaster is applied and cured on a porous substrate, the porous network changes along the thickness and namely at the interface, which in turn influences the drying behaviour of the entire system. The results indicated that the addition of linseed oil to the lime plaster has negatively influenced the bonding process thus creating an hydraulic resistivity for the moisture to flow from the brick to the plaster during drying. This phenomena can be mainly atributed to three factors: i) hydrophobization of part of the mortar pores; ii) the development of air bubbles related to entrained air during the mixing process; and iii) the mismatch between the physical-chemical properties of both systems (brick and plaster), namely the different pore network and surface energy (water-repellent effect), which affects the interpenetration of both porous layers. On the other hand, the formation of air voids promoted by the addition of linseed oil to the lime plasters inhibits the development of shrinkage cracks.

We can conclude that investigating only the drying kinetics of mono-material plaster specimens can lead to erroneous conclusions and recommendations for practical applications. Drying processes are particularly significant in conditioning damage when soluble salts are present because during drying salts migrate in the porous materials and crystallisation eventually takes place on the surface (efflorescence) or in the pores (subflorescence) of the materials. The study of how the drying behaviour varies when we have a salt solution instead of pure water will be presented in a future publication.

Acknowledgements

The NMR measurements were performed at the Department of Applied Physics in TU/e at the group of Transport in Permeable Media. The remaining experimental work was carried out at ITAM. This study was supported by the project LO1219 of the Ministry of Education, Youth and Sports of the Czech Republic, National Sustainability Programme I. We thank Jef Noijen, Hans Dalderop and Pim Donkers for their assistance with the NMR experiments, and Veronika Petráňová, Krzysztof Niedoba, and Vladimír Novák for helping with the SEM, MIP, and thin sections' preparation, respectively.

References

[1] S. Pavía, B. Fitzgeral, E. Treacy, An assessment of lime mortars for masonry repair, in: Ciaran McNally (Ed.), Concrete Research in Ireland Colloquium, University College Dublin, 2006, pp. 101–108.
[2] R.P.J. van Hees, L. Binda, I. Papayianni, E. Toumbakari, Characterisation and damage analysis of old mortars, Mater. Struct. 37 (2004) 644–648, http://dx.doi.org/10.1007/bf02483293.

[3] A.C. Magalhães, M.R. Veiga, F. Cartaxo, Characterization of lime mortars with water repellent for use on ancient building's walls, in: Proc. 7th Int. Masonry Conference 7IBMAC, 2006.
[4] A. Izaguirre, J. Lanas, J.I. Álvarez, Effect of water-repellent admixtures on the behaviour of aerial lime-based mortars, Cem. Concr. Res. 39 (2009) 1095–1104, http://dx.doi.org/10.1016/j.cemconres.2009.07.026.
[5] L. Falchi, U. Müller, P. Fontana, F.C. Izzo, E. Zendri, Influence and effectiveness of water-repellent admixtures on pozzolana-lime mortars for restoration application, Constr. Build. Mater. 49 (2013) 272–280, http://dx.doi.org/10.1016/j.conbuildmat.2013.08.030.
[6] L.B. Sickels, Organic additives in mortars, Edinburgh: Edinburgh Archit. Res. 8 (1981).
[7] A.F.G. Sá, Renders in Walls of Lime and Stone (in Portuguese) MSc thesis, IST, Lisbon, 2005.
[8] L. Ventolà, M. Vendrell, P. Giraldez, L. Merino, Traditional organic additives to improve lime mortars: new old materials for restoration and building natural stone fabrics, Constr. Build. Mater. 25 (2011) 3313–3318, http://dx.doi.org/10.1016/j.conbuildmat.2011.03.020.
[9] C.C. Santiago, M. Mendonca de Oliveira, Organic additives in Brazilian lime mortars, in Lime and other alternative cements, in: N. Hill, S. Holmes, D. Mather (Eds.), Intermediate Technology Publications, London, 1992, http://dx.doi.org/10.3362/9781780442631.013. 178–176.
[10] S.Q. Fang, H. Zhang, B. Zhang, G. Li, A study of Tung-oil-lime putty: a traditional lime-based mortar, Int. J. Adhes. Adhes. 48 (2014) 224–230, http://dx.doi.org/10.1016/j.ijadhadh.2013.09.034.
[11] E. Čechová, The Effect of Linseed Oil on the Properties of Lime-Based Restoration Mortars PhD thesis, Università di Bologna, Bologna, 2009.
[12] E. Vejmelková, M. Keppert, P. Rovnaníková, Z. Keršner, R. Černý, Properties of lime composites containing a new type of pozzolana for the improvement of strength and durability, Composites Part B 43 (2012) 3534–3540, http://dx.doi.org/10.1016/j.compositesb.2011.11.053.
[13] E. Vejmelková, D. Koňáková, M. Čáchová, M. Keppert, R. Černý, Effect of hydrophobization on the properties of lime-metakaolin plasters, Constr. Build. Mater. 37 (2012) 556–561, http://dx.doi.org/10.1016/j.conbuildmat.2012.07.097.
[14] T.D. Gonçalves, L. Pel, J. Delgado Rodrigues, Worsening of dampness and salt damage after restoration interventions: use of water-repellent additives in plasters and renders, in: Proc. HMC08, LNEC, Lisbon, 2008.
[15] C. Hall, W.D. Hoff, Water transport in brick, stone and concrete, second ed., CRC Press, New York, 2012, http://dx.doi.org/10.4324/9780203301708.
[16] I.I. Rilem, 5, Evaporation curve, RILEM 25-PEM, Matér. Constr. 75 (13) (1980) 205–207.
[17] N. Shahidzadeh-Bonn, A. Azouni, P. Coussot, Effect of wetting properties on the kinetics of drying of porous media, J. Phys.: Condens. Matter 19 (2007) 112101, http://dx.doi.org/10.1088/0953-8984/19/11/112101.
[18] C. Nunes, Z. Slížková, Hydrophobic lime based mortars with linseed oil: characterisation and durability assessment, Cem. Concr. Res. 61–62 (2014) 28–39, http://dx.doi.org/10.1016/j.cemconres.2014.03.011.
[19] H. Brocken, Moisture Transport in Brick Masonry: The Grey Area between Bricks Ph.D. thesis, TU/e, Eindhoven, 1998.
[20] L. Pel, H. Brocken, K. Kopinga, Determination of moisture diffusivity in porous media using moisture concentration profiles, Int. J. Heat Mass Transfer 39 (1996) 1273–1280, http://dx.doi.org/10.1016/0017-9310(95)00201-4.
[21] H. Brocken, O.C.G. Adan, L. Pel, Moisture transport properties of mortar and mortar joints: a NMR study, Heron 42 (1997) 55–69.
[22] H. Brocken, M.E. Spiekman, L. Pel, K. Kopinga, J.A. Larbi, Water extraction out of mortar during brick laying: a NMR study, Mater. Struct. 31 (1998) 49–57, http://dx.doi.org/10.1007/bf02486414.
[23] J. Petkovic, H.P. Huinink, L. Pel, K. Kopinga, R.P.J. Van Hees, Salt transport in plaster/substrate layers, Mater. Struct. 40 (2007) 475–490, http://dx.doi.org/10.1617/s11527-006-9151-7.
[24] T.D. Gonçalves, Salt crystallization in plastered or rendered walls Ph.D. thesis, IST, Lisbon, 2007.
[25] S. Diamond, Mercury porosimetry: an inappropriate method for the measurement of pore size distributions in cement-based materials, Cem. Concr. Res. 30 (2000) 1517–1525, http://dx.doi.org/10.1016/S0008-8846(00)00370-7.
[26] S. Wild, A discussion of the paper "Mercury porosimetry—an inappropriate method for the measurement of pore size distributions in cement-based materials" by S. Diamond, Cem. Concr. Res. 31 (2001) 1653–1654, http://dx.doi.org/10.1016/S0008-8846(01)00616-0.
[27] M. Thomson, Porosity of mortars, in: C. Groot, G. Ashall, J. Hughes (Eds.), Characterisation of Old Mortars with Respect to their Repair, RILEM TC 167-COM, Springer, New York, 2004, pp. 77–106, http://dx.doi.org/10.1617/2912143675.006.
[28] J. Elsen, Microscopy of historic mortars – a review, Cem. Concr. Res. 36 (2006) 1416–1424, http://dx.doi.org/10.1016/j.cemconres.2005.12.006.
[29] M. Stefanidou, L. Papadopoulou, E. Pavlidou, I. Papayianni, Applying microscopic techniques for the investigation of the behaviour of building materials, in: A. Méndez-Vilas (Ed.), Microscopy: Advances in Scientific Research and Education, vol. 2, Formatex Research Center, Badajoz, 2014, pp. 1064–1070.
[30] K. Kopinga, L. Pel, One dimensional scanning of moisture in porous materials with NMR, Rev. Sci. Instrum. 65 (1994) 3673–3681, http://dx.doi.org/10.1063/1.1144491.
[31] R.M.E. Valckenborg, L. Pel, K. Hazrati, K. Kopinga, J. Marchand, Pore water distribution during drying as determined by NMR, Mater. Struct. 34 (2001) 599–604, http://dx.doi.org/10.1007/bf02482126.
[32] BS EN 459–1, Building lime. Definitions, specification and conformity criteria, 2015. http://dx.doi.org/10.3403/00489688u.
[33] UNE-EN 1015–2. Methods of test for mortar for masonry, Part 3: Determination of consistency of fresh mortar, 1999. http://dx.doi.org/10.3403/01541440.
[34] J. Rouquerol, D. Avnir, C.W. Fairbridge, D.H. Everett, J.H. Haynes, N. Pernicone, J.D.F. Ramsay, K.S.W. Sing, K.K. Unger, Recommendations for the characterization of porous solids, Pure Appl Chem 66 (8) (1994) 1739–1758, http://dx.doi.org/10.1351/pac199466081739.
[35] L. Pel, P.A.J. Donkers, K. Kopinga, J.J. Noijen, ^{1}H, ^{23}Na and ^{35}Cl imaging in cementitious materials with NMR, Appl. Magn. Reson. 47 (2016) 265–276, http://dx.doi.org/10.1007/s00723-015-0752-6.
[36] S. Gupta, H.P. Huinink, M. Prat, L. Pel, K. Kopinga, Paradoxical drying of a fired-clay brick due to salt crystallization, Chem. Eng. Sci. 109 (2014) 204–211, http://dx.doi.org/10.1016/j.ces.2014.01.023.
[37] R.M.E. Valckenborg, L. Pel, K. Kopinga, Combined NMR cryoporometry and relaxometry, J. Phys. D Appl. Phys. 35 (2002) 249–256, http://dx.doi.org/10.1088/0022-3727/35/3/314.
[38] W. Kurdowski, Cement and Concrete Chemistry, Springer Science & Business, 2014, http://dx.doi.org/10.1007/978-94-007-7945-7.
[39] H. Justnes, T.A. Ostnor, B. Vila, Vegetable oils as water-repellents for mortars, in: Proc. 1st Int. Conf. Asian Concrete Federation, Chiang Mai, 2004, pp. 689–698.
[40] S. Roels, J. Elsene, J. Carmeliet, H. Hens, Characterisation of pore structure by combining mercury porosimetry and micrography, Mater. Struct. 34 (2001) 76–82, http://dx.doi.org/10.1007/bf02481555.
[41] P.A.C. Gane, C.J. Ridgway, E. Lehtinen, R. Valiullin, I. Furó, J. Schoelkopf, H. Paulapuro, J. Daicic, Comparison of NMR cryoporometry, mercury intrusion porosimetry, and DSC thermoporosimetry in characterizing pore size distributions of compressed finely ground calcium carbonate structures, Ind. Eng. Chem. Res. 43 (2004) 7920–7927, http://dx.doi.org/10.1021/ie049448p.
[42] V. Nežerka, Z. Slížková, P. Tesárek, T. Plachý, D. Frankeová, V. Petráňová, Comprehensive study on mechanical properties of lime-based pastes with additions of metakaolin and brick dust, Cem. Concr. Res. 64 (2014) 17–29, http://dx.doi.org/10.1016/j.cemconres.2014.06.006.
[43] P. Schubert, Shrinkage behaviour of aerated concrete, in F.H. Wittman (Ed.) Autoclaved concrete, moisture and properties. Amsterdam: Elsevier, 1983, 207–217 as cited by N. Narayanan, K. Ramamurthy (2000) Structure and properties of aerated concrete: A review, Cem Concr Comp 22, 321–329.
[44] L. Pel, K. Kopinga, H. Brocken, Moisture transport in porous building materials, Heron 41 (2) (1996) 95–105.
[45] L. Pel, A.A.J. Ketelaars, O.C.G. Adan, A.A. Van Well, Determination of moisture diffusivity in porous media using scanning neutron radiography, Int. J. Heat Mass Transfer 36 (1993) 1261–1267, http://dx.doi.org/10.1016/s0017-9310(05)80095-x.
[46] L. Pel, Moisture Transport in Porous Building Materials Ph.D. thesis, TU/e, Eindhoven, 1995.
[47] G.W. Scherer, Theory of drying, J. Am. Ceram. Soc. 73 (1990) 3–14, http://dx.doi.org/10.1111/j.1151-2916.1990.tb05082.x.
[48] E. Keita, P. Faure, S. Rodts, P. Coussot, D.A. Weitz, Evaporation from a capillary tube: experiment and modelisation, in: Proc. 5th Int. Conf. Porous Media and its Applications in Science and Engineering ICPM5, Kona, 2014.
[49] C. Nunes, Z. Slížková, D. Křivánková, Lime-based mortars with linseed oil: sodium chloride resistance assessment and characterization of the degraded material, Per Mineralogia 82 (3) (2013) 411–427, http://dx.doi.org/10.2451/2013pm0024.
[50] C. Groot, Effect of water on mortar-brick bond Ph.D. thesis, TUDelft, Delft, 1993.
[51] R.S. Boyton, K.A. Gutschick, Bond of Mortar to Masonry Units, National Lime Association, Washington D.C., 1975.
[52] V.P. de Freitas, V. Abrantes, P. Crausse, Moisture migration in building walls – analysis of the interface phenomena, Build. Environ. 31 (2) (1996) 99–108, http://dx.doi.org/10.1016/0360-1323(95)00027-5.
[53] N. Shokri, P. Lehmann, D. Or, Effects of hydrophobic layers on evaporation from porous media, Geophys. Res. Lett. 35 (2008) L19407, http://dx.doi.org/10.1029/2008gl035230.
[54] D.H. Kim, H.J. Yang, K.Y. Kim, T.S. Yun, Experimental investigation of evaporation and drainage in wettable and water-repellent sands, Sustainability 7 (2015) 5648–5663, http://dx.doi.org/10.3390/su7055648.
[55] R. Wua, G.-M. Cui, R. Chen, Pore network study of slow evaporation in hydrophobic porous media, Int. J. Heat Mass Transfer 68 (2014) 310–323, http://dx.doi.org/10.1016/j.ijheatmasstransfer.2013.09.042.